AIP Journal of Applied Physics

Influence of wetting layers and quantum dot size distribution on intermediate band formation in InAs/GaAs superlattices

S. Huang, A. V. Semichaevsky, L. Webster, H. T. Johnson, and R. S. Goldman

Citation: J. Appl. Phys. **110**, 073105 (2011); doi: 10.1063/1.3631785
View online: http://dx.doi.org/10.1063/1.3631785
View Table of Contents: http://jap.aip.org/resource/1/JAPIAU/v110/i7
Published by the AIP Publishing LLC.

Additional information on J. Appl. Phys.

Journal Homepage: http://jap.aip.org/
Journal Information: http://jap.aip.org/about/about_the_journal
Top downloads: http://jap.aip.org/features/most_downloaded
Information for Authors: http://jap.aip.org/authors

ADVERTISEMENT

Downloaded 28 Jun 2013 to 141.211.173.82. This article is copyrighted as indicated in the abstract. Reuse of AIP content is subject to the terms at: http://jap.aip.org/about/rights_and_permissions

JOURNAL OF APPLIED PHYSICS 110, 073105 (2011)

Influence of wetting layers and quantum dot size distribution on intermediate band formation in InAs/GaAs superlattices

S. Huang,[1] A. V. Semichaevsky,[2,a)] L. Webster,[3] H. T. Johnson,[2] and R. S. Goldman[1,3]
[1]*Department of Materials Science and Engineering, University of Michigan, Ann Arbor, Michigan 48109, USA*
[2]*Department of Mechanical Science and Engineering, University of Illinois, Urbana, Illinois 61801, USA*
[3]*Applied Physics Program, University of Michigan, Ann Arbor, Michigan 48109, USA*

(Received 13 July 2011; accepted 31 July 2011; published online 4 October 2011)

We examine the influence of the wetting layers (WLs) and the quantum dot (QD) size distribution on the sub-bandgap external quantum efficiency (EQE) of QD solar cells. We use a finite-element Schrödinger-Poisson model that considers QD and wetting layer shapes, sizes, and spacings from cross-sectional scanning tunneling and atomic force micrographs. A comparison between experiments and computations reveals an insignificant contribution of the WL to the sub-bandgap EQE and a broadening of sub-bandgap EQE associated with a variation in QD sizes in the growth direction. © *2011 American Institute of Physics*. [doi:10.1063/1.3631785]

I. INTRODUCTION

Quantum dot (QD) superlattices (SLs) have been proposed for improving solar cell efficiency by providing intermediate energy bands to allow sub-bandgap photon absorption,[1,2] thereby enhancing the photocurrent.[3] Although photocurrent enhancement from QD-based solar cells has been demonstrated,[3–15] QD cells have consistently exhibited lower open-circuit voltages (V_{OC}) and conversion efficiencies than the GaAs reference cells. The QD cells to date have involved "zero-dimensional" structures produced using the Stranski-Krastanov (SK) growth process. SK QD structures have been reported to contain two-dimensional wetting layers (WLs)[16] and a distribution of QD sizes,[17] which are expected to influence the energies and broadening of the intermediate bands (IBs). A comparison of the properties of *p-i-n* heterostuctures containing either SK InAs QDs or thin InAs layers reveals insignificant sub-bandgap external quantum efficiency (EQE) due to the WL in comparison with cells containing only QDs.[12] A comparison of calculated energy level splittings for a vertically aligned pair of InAs QDs in a GaAs matrix with identical or variable sizes in adjacent layers reveals a more significant level splitting for the QD pair with size variation.[18] However, the influence of the WL and the QD size variation on the EQE of *p-i-n* heterostructures containing multilayer QD arrays has not yet been reported.

Here, we examine the relative influence of the WL and the QD size distribution on the sub-bandgap EQE of molecular beam epitaxially (MBE) grown QD solar cells. Realistic QD shapes, sizes, and SL vertical periods from cross-sectional scanning tunneling microscopy (XSTM) and areal densities from atomic force microscopy (AFM) are used as input into finite-element Schrödinger-Poisson calculations of the EQE. A comparison between experiments and simulations reveals a broadening of sub-bandgap EQE associated with a variation in QD sizes in the growth direction and an insignificant contribution of the WL to the sub-bandgap EQE. This unique combination of experiment and theory provides new insight for designing QD SLs for a wide variety of applications.

II. EXPERIMENTAL PROCEDURES

The heterostructures were grown on Zn-doped *p*-GaAs (001) substrates by MBE, using solid Ga, Be, Si, Al, In, and As_2 sources. The target doping concentrations were $\sim 1 \times 10^{18}$ cm^{-3} for both *p*- and *n*-type layers. An initial 250-nm-thick Be-doped *p*-GaAs and a 500-nm-thick undoped GaAs buffer layer were grown at 580 °C, followed by a 20-nm-thick undoped GaAs layer grown at 500 °C, both with a V:III ratio of 12:1. Subsequently, three-period InAs/GaAs QD SLs consisting of 2.6 monolayers (MLs) of InAs and a 5 nm GaAs spacer were grown at 500 °C.[19] This approach is expected to lead to the formation of QDs via a SK growth mode transition. For the *p-i-n* structure, the final QD layer was capped with a 500-nm-thick layer of undoped GaAs. Next, layers of 200-nm-thick *n*-GaAs, 50-nm-thick $Al_{0.3}Ga_{0.7}As$, and 20-nm-thick heavily doped *n*-GaAs were then grown in succession. For the control *p-i-n* heterostructures, 15-nm-thick GaAs layer was grown instead of the QD layers. To reduce the quasi-Fermi level discontinuities within the QD SL, a total *i*-layer thickness of >1 μm were utilized. 2×2 mm^2 cells without anti-reflection coatings were fabricated using standard photolithography with front Ge/Ni/Au n-type and back Au/Zn p-type contacts deposited by e-beam evaporation. The front contact shadowing was ∼6% of the surface area.

The EQE as a function of wavelength (λ) was measured with a halogen lamp calibrated with a National Institute of Standards and Technology traceable silicon photodetector. Low-intensity illumination ($\ll$100 mW/cm^2) from the halogen lamp was modulated by a chopper, spectrally filtered with a monochromator, and guided via an optical fiber to the sample. The photocurrent was then measured at room temperature using a lock-in amplifier referenced to the chopper

[a)]Author to whom correspondence should be addressed. Electronic mail: avsemych@uiuc.edu.

 © 2011 American Institute of Physics

Downloaded 28 Jun 2013 to 141.211.173.82. This article is copyrighted as indicated in the abstract. Reuse of AIP content is subject to the terms at: http://jap.aip.org/about/rights_and_permissions

frequency. AFM was performed on samples grown with similar conditions except that the final QD layer was left uncapped. XSTM measurements were obtained on samples grown in a similar manner but with five-period InAs/GaAs QD SLs on n-GaAs and capped with n-GaAs. To differentiate the GaAs and QDs within the XSTM images, we estimated the top height criterion as follows. Bright regions protruding at least 4.2 Å above the GaAs background were assessed as possible QDs. Within the bright regions, pixels with tip heights of at least 1.8 Å above the GaAs background were considered to be part of the QD.[20] We examined several high resolution XSTM images and obtained QD height and lateral size distributions from more than 100 QDs.

III. FINITE-ELEMENT SCHRÖDINGER-POISSON CALCULATIONS

To calculate the EQE enhancement due to the presence of the QDs, we use a finite-element solution of the Poisson (1) and Schrödinger (2) equations. The Schrödinger equation includes a confining potential, V_0, that accounts for the influence of misfit strain, and the electric potential Φ.

$$\nabla^2\Phi = -\frac{\rho}{\varepsilon_0\varepsilon}, \tag{1}$$

$$-\frac{\hbar^2}{2m^*}\nabla^2\Psi + (e\Phi + V_0)\Psi = \Lambda\Psi, \tag{2}$$

where ρ is the charge density, ε is the permittivity, Ψ are the wave functions, Λ are the eigenstates, m^* is the carrier effective mass, and e is the electron charge. The Poisson equation, coupled to the diffusion equations for the electrons and holes, is first solved on the scale of the whole p-i-n structure, and thus, the position-dependent built-in potential can be determined. The value of the built-in electric field in the heterostructure region is found to be $\sim 7.5\times10^5$ V/m. The charge density in Eq. (1) is calculated for the p-i-n structure described above, using literature values for the carrier mobilities, with $\phi = 0$ defined as the Fermi level of the bottom GaAs layer.

We consider In-Ga interdiffusion in the WLs based upon an analysis of XSTM data from Ref. 16. Thus, the position-dependent In concentration in the wetting layer, x_{In}, is approximated by a Gaussian profile, $x_{In} = 0.32\exp(-(z-z_{0i})^2/\sigma^2)$, where z_{0i} is the position in the middle of the ith QD layer along the growth (z-) direction, and σ is the standard deviation, which equals 1.25 nm. We take the inhomogeneous In concentration[16] into account via the linear combination of carrier effective masses, so that the effective mass of the alloy is position-dependent, $m^*(z)$ in Eq. (2), given by

$$m^*(z) = x_{In}(z)m^*_{In} + (1 - x_{In}(z))m^*_{Ga}, \tag{3}$$

The mechanical strain field in the QDs and WLs is found numerically using a finite-element continuum elasticity model, with QD dimensions and x_{In} from an analysis of XSTM data. The lattice constants in the inhomogeneous WLs are then determined using Vegard's law, as follows:

$$a(z) = x_{In}(z)a_{In} + (1 - x_{In}(z))a_{Ga}, \tag{4}$$

The strain-modified band offsets, which we use to determine the confining potential profile for the QD heterostructure, are determined using deformation potentials from the literature.[21]

Using the valence and (conduction) band wave functions Ψ_n (Ψ_k), and energy levels E_n (E_k), at photon momentum $q = 0$, the optical absorption spectrum of a QD becomes

$$\begin{aligned}\alpha_{QD}(\omega) = {} & \frac{2}{\sqrt{2\pi}\sigma}\sqrt{\frac{\mu}{\varepsilon}}\frac{\hbar^2\pi}{V}\left(\frac{e}{m_0}\right)^2 A^2 \int\sum_{n,k}\frac{\hbar}{E_k - E_n} \\ & \times\left\{\left|\int_V \Psi_k^*(0,\vec{r})\left(\frac{\partial}{\partial x}\Psi_n(0,\vec{r})\right)d^3\vec{r}\right|^2\right. \\ & \left.+\left|\int_V \Psi_k^*(0,\vec{r})\left(\frac{\partial}{\partial y}\Psi_n(0,\vec{r})\right)d^3\vec{r}\right|^2\right\}(f(E_n)-f(E_k)) \\ & \times\exp\{-(E-\hbar\omega)^2)/2\sigma^2\}dE,\end{aligned} \tag{5}$$

where μ and ε are material permeability and permittivity, respectively; n and k are the indices of the initial and final confined states, $f(E)$ is the electronic occupancy given by the Fermi distribution, assuming that the Fermi level is in the middle of the bulk GaAs bandgap, σ is thermal broadening (0.026 eV at room temperature), V is the unit cell volume, and $A = 1$ (1/3) for heavy (light) holes. The net effective absorption of a unit cell containing QDs is then determined using the volumetric average of the combined heavy and light hole absorption in the QDs and the absorption in the GaAs barrier.[22]

The absorption coefficients, refractive indices, carrier effective masses, and carrier diffusion lengths of GaAs are taken from literature reports.[23] For the typical QD densities in our samples, the lateral spacing between QDs is on the order of 40 to 90 nm. Based on the solution of the Schrödinger equation, at such a large lateral separation between the dots, it is reasonable to assume that the overlap integrals between the wave functions of electrons in these dots are negligibly small, and the lateral coupling between QDs will not contribute significantly to the miniband broadening. The tunneling transmission coefficient between states in vertically stacked QDs for the confined electrons at the top of the potential well is $T \approx 16\exp\left(-2a\sqrt{2m^*V_0/\hbar^2}\right) < 10^{-4}$, where a is the spacing between the QDs in adjacent layers. For the calculations, we consider an array of QDs infinitely periodic in x and y, arranged in three period SLs along the z-(growth) axis.

The EQE of the device is calculated from the short-circuit photocurrent density at the i-p interface. The steady-state photogeneration-drift-diffusion equations are solved for the electron current density on the p-side of the i-p interface, neglecting the dark current. The photocurrent density is normalized to the incident solar photon flux $\Phi_{inc}(\lambda)$, according to

$$\begin{aligned}EQE(\lambda) = \frac{1}{F_{inc}(\lambda)}\Bigg\{ & \int_{-W_n}^{W_i} F(\lambda,z)\alpha(\lambda,z)dz \\ & + F(\lambda,W_i)\frac{\alpha(\lambda,W_i)L_n}{1+\alpha(\lambda,W_i)L_n}\Bigg\},\end{aligned} \tag{6}$$

Downloaded 28 Jun 2013 to 141.211.173.82. This article is copyrighted as indicated in the abstract. Reuse of AIP content is subject to the terms at: http://jap.aip.org/about/rights_and_permissions

where L_n is the electron diffusion length in the *p*-region, $F(\lambda, z)$ is the photon flux traversing the plane at position z in the intrinsic region, $\alpha(\lambda, z)$ is the absorption coefficient of either the bulk or the QD-doped semiconductor, W_i and W_n are the thicknesses of the intrinsic and *n*-type layers, respectively, and $F_{inc}(\lambda)$ is the incident (solar) photon flux. The position $z = 0$ corresponds to the position of the *n-i* interface. A transfer matrix approach is used to calculate the propagation of randomly polarized solar illumination normally incident on the *p-i-n* structure.

IV. RESULTS AND DISCUSSION

Figure 1(a) shows an AFM image of an InAs/GaAs QD SL, with QD density of $\sim 1.0 \times 10^{10}$ cm^{-2}. Figure 1(b) shows a representative XSTM image of the QD SLs. In Fig. 1(b), fringes with a spacing of 5.65 and 6.06 Å, corresponding to the (001) planes of GaAs and InAs, respectively, are observed in the darker and brighter regions of the image. The distribution of QD sizes, estimated from several high resolution XSTM images, is presented in Fig. 2 for each period of QDs. We fit the size distributions with a Gaussian distribution for QD frequency as a function of diameter (or height) and used the maximum likelihood estimation method to obtain the most probable QD diameter (or height).[24] For the 1st, 2nd, and 3rd period of QDs, the maximum likelihood diameters (heights), d_{ML} (h_{ML}), are 12.0 ± 0.5, 15.9 ± 0.5, and 19.4 ± 0.5 nm (3.5 ± 0.3, 3.8 ± 0.3, and 4.1 ± 0.3 nm), respectively.

To compute the optical absorption and EQE of the 3-period QD SLs, we assume axially-symmetric ellipsoids with d_{ML} and h_{ML} as defined in Fig. 2, and 100 nm (5.8 nm) lateral (vertical) SL periods. We then compare the experimental and computed EQEs for the following configurations: three SLs containing identically sized QDs with diameter (height) of 12.0 (3.5) nm, 15.9 (3.8) nm, and 19.4 (4.1) nm without WLs; SLs with increasing QD sizes in the subsequent layers, as listed in Table I, embedded in either GaAs or $In_xGa_{1-x}As$ WLs; and SL with three period of WLs only.

To consider the effect of QD size variations, we compare the calculated EQEs for SLs containing identically sized QDs without WLs. The calculated EQEs are plotted in Fig. 3(a), where the additional spectral response at wavelengths longer than the GaAs absorption edge (at $\lambda = 870$ nm) is apparent for all SLs.

To quantify the position of sub-bandgap EQE peak, we consider the first moment of the calculated sub-bandgap

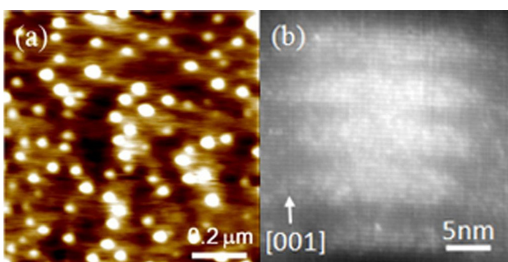

FIG. 1. (Color online) (a) AFM image of InAs/GaAs QD SLs grown on GaAs buffer layers. (b) High-resolution XSTM topographic image of InAs/GaAs QD SLs.

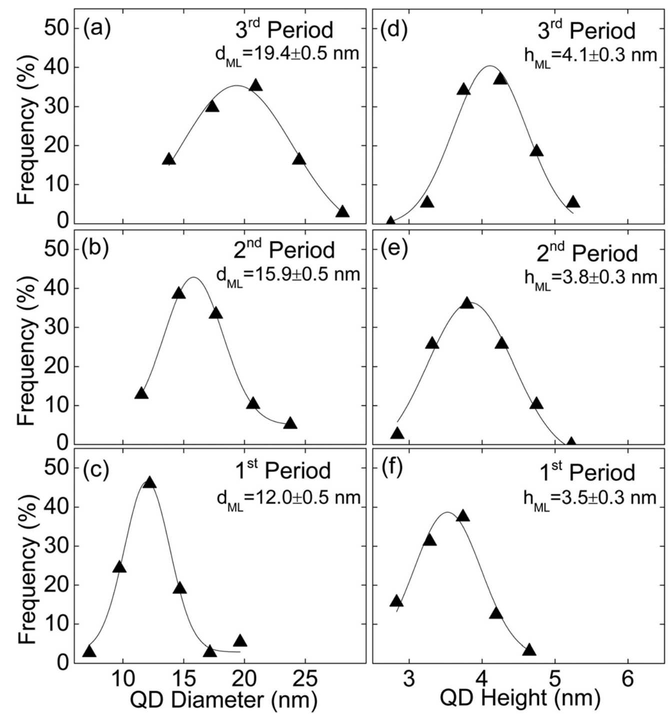

FIG. 2. (a)-(f) The in-plane diameter and height distributions for each period of QDs determined from an analysis of XSTM images. The Frequency is the percentage of QDs with diameters or heights within a specified range. Fits to a Gaussian distribution are shown as solid lines, with χ values (a) 0.93, (b) 0.99, (c) 0.98, (d) 0.93, (e) 0.95, and (f) 0.88. For the 1st, 2nd, and 3rd period of QDs, a maximum likelihood estimate of QD diameters (heights) gives d_{ML} (h_{ML}) values of 12.0 ± 0.5, 15.9 ± 0.5, and 19.4 ± 0.5 nm (3.5 ± 0.3, 3.8 ± 0.3, and 4.1 ± 0.3 nm), respectively.

EQE(λ), which is an integral of the EQE weighted by the wavelength, normalized by the integral of the EQE, $m = \int_{\lambda_1}^{\lambda_2} EQE(\lambda)\lambda d\lambda / \int_{\lambda_1}^{\lambda_2} EQE(\lambda)d\lambda$, where $\lambda_1 = 870$ nm and $\lambda_2 = 1100$ nm. Here, m = 910, 916, and 932 nm for a SL with QD diameters of 19.4, 15.9, and 12.0 nm, respectively. Due to the reduction in QD volumetric fraction and average transition matrix element, the calculated EQE is reduced from 1.44% to 0.6% as QD diameter decreases from 19.4 to 12 nm.

For a fixed QD aspect ratio, the sub-bandgap EQE is expected to blue-shift with the decreasing QD size due to stronger quantum confinement. However, we do not observe a clear trend in the sub-bandgap EQE as QD size decreases. This is due to the effect of aspect ratio of the ellipsoidal QDs on quantum confinement and the attendant variation in interlayer spacing. The results shown in Fig. 3(a) are based on matching QD geometry as closely as possible to the experimental morphology; some insight into the related effect of the optical bandgap variation with QD interlayer spacing is provided in Ref. 25.

TABLE I. Dimensions of the InAs QDs determined from an analysis of XSTM images.

Period	Height (nm)	Diameter (nm)
3rd	4.1	19.4
2nd	3.8	15.9
1st	3.5	12.0

Downloaded 28 Jun 2013 to 141.211.173.82. This article is copyrighted as indicated in the abstract. Reuse of AIP content is subject to the terms at: http://jap.aip.org/about/rights_and_permissions

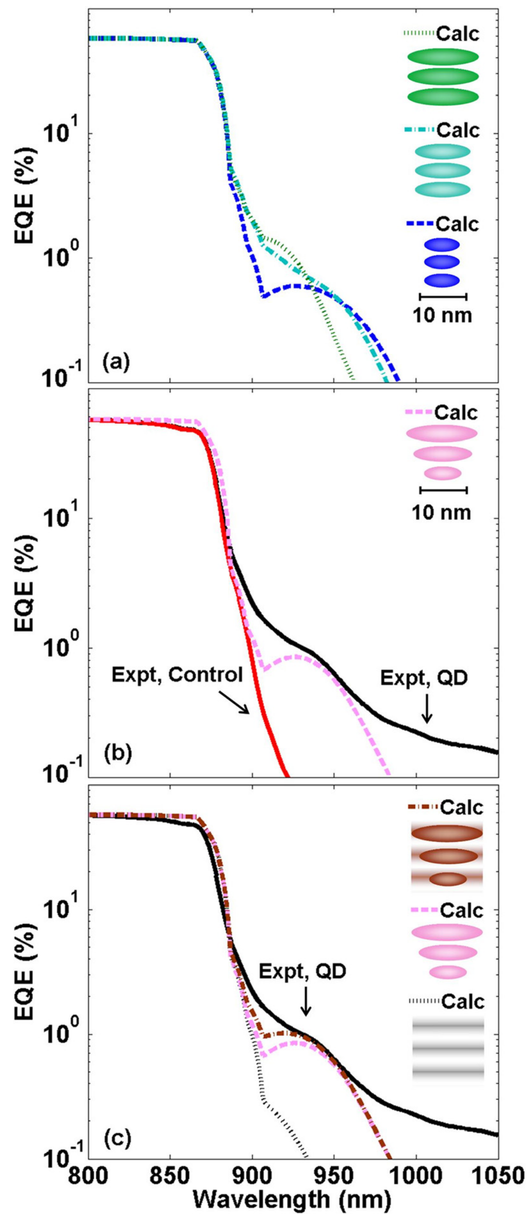

FIG. 3. (Color online) Plots of (a) computed EQE vs. wavelength (λ) for three SLs containing identically-sized QDs without WLs. The input values of the QD diameters (heights), determined from an analysis of XSTM images, are 12.0 (3.5) nm, 15.9 (3.8) nm, and 19.4 (4.1) nm; (b) measured EQE vs. λ for the QD and control cells, along with the calculated EQE vs. λ values for QD SL with vertical size variations; and (c) measured EQE vs. λ for the QD cell, along with the computed EQE vs. λ values for the QD SLs with vertical size variations and WLs, the QD SLs with vertical size variation, but without WLs, and the WLs without QDs.

We have also examined the influence of vertical variations in QD sizes by comparing the calculated EQE for QD SL with variations in QD sizes between layers along the vertical growth direction with the experimental EQEs of the control and QD cells, as shown in Fig. 3(b). The calculated EQEs in Fig. 3(b) exhibit a broad sub-bandgap EQE extension similar to that of the measured EQE of the QD cell. The first moment of the calculated EQE for the QD SL with varying diameters, $m = 927$ nm, also agrees well with the experimental value of 922 nm.

To account for the WL contributions to the sub-bandgap EQE, we compare the measured EQE of the QD cell with the calculated EQEs of (1) SL with WLs only and SLs with vertical QD size variation (2) without and (3) with WLs, as shown in Fig. 3(c). When WLs are included in the SL, the calculated EQE = 1.02% at $\lambda = 920$ nm (the wavelength corresponding to the first moment of the sub-bandgap EQE), which leads to improved agreement with the measured value of 1.04%. The small discrepancy might be due to additional spectral broadening of photocurrent response resulting from in-plane QD size distributions. In addition, the WL contribution to the sub-bandgap EQE is insignificant in comparison to that of the QDs. At $\lambda = 920$ nm, the calculated WL EQE = 0.17%, while the QD EQE = 0.82%. This is consistent with the measured EQE for which a peak associated with the WL is not apparent. The WL contribution is insignificant due to its low strain-induced confinement potentials (~41 meV for the maximum CB potential; ~8 mV for the VB), small average matrix element, and low interband absorption strength.

V. CONCLUSIONS

In summary, we have studied the influence of WL and QD size variation on sub-bandgap EQE of QD solar cells using a finite-element Schrödinger-Poisson model that considers realistic QD sizes and shapes obtained from MBE-grown InAs QD on GaAs structures. A comparison between experiment and simulation reveals a broadening of sub-bandgap EQE associated with a variation in QD sizes in the growth direction. Furthermore, the inhomogeneous WL contribution to the sub-bandgap EQE is predicted to be much weaker than that of the QD SLs.

ACKNOWLEDGMENTS

We gratefully acknowledge partial support of the National Science Foundation through Grant No. CBET 09-33348. AVS, HTJ, and LW were supported in part by DOE-BES Grant No. DE-FG02-06EF46339. SH and RSG were supported by the Center for Solar and Thermal Energy Conversion, an Energy Frontier Research Center funded by the U.S. Department of Energy, Office of Science, Office of Basic Energy Sciences under Award Number DE-SC0000957. Authors SH and AVS contributed equally to this work. The authors would like to thank Kuen-Ting Shiu and Kyusang Lee for assistance with device fabrication and measurements.

[1]A. Luque and A. Marti, Phys. Rev. Lett. **78**, 5014 (1997).
[2]A. S. Brown and M. A. Green, J. Appl. Phys. **94**, 6150 (2003).
[3]S. M. Hubbard, C. Bailey, S. Polly, C. Cress, J. Andersen, D. Forbes, and R. Raffaelle, J. Nanophotonics **3**, 031880 (2009).
[4]A. J. Grenko, I. Kimukin, J. Walker, and E. Towe, *Solar Energy: New Materials and Nanostructured Devices for High Efficiency (Solar)* (Stanford University, California, 2008), p. SWA4.
[5]A. Luque, A. Martí, N. López, E. Antolín, E. Cánovas, C. Stanley, C. Farmer, L. J. Caballero, L. Cuadra, and J. L. Balenzategui, Appl. Phys. Lett. **87**, 083505 (2005).
[6]S. A. Blokhin, A. V. Sakharov, A. M. Nadtochy, A. S. Pauysov, M. V. Maximov, N. N. Ledentsov, A. R. Kovsh, S. S. Mikhrin, V. M. Lantratov, S. A. Mintairov, N. A. Kaluzhniy, and M. Z. Shvarts, Semiconductors **43**, 514 (2009).
[7]A. G. Norman, M. C. Hanna, P. Dippo, D. H. Levi, R. C. Reedy, J. S. Ward, and M. M. Al-Jassim, *Proceedings of the 31st IEEE Photovoltaic*

Downloaded 28 Jun 2013 to 141.211.173.82. This article is copyrighted as indicated in the abstract. Reuse of AIP content is subject to the terms at: http://jap.aip.org/about/rights_and_permissions

Specialists Conference (IEEE Electron Device Society (IEEE EDS), Lake Buena Vista, Florida, 2005), pp. 43–48.
[8]C. O. McPheeters, C. J. Hill, S. H. Lim, D. Derkacs, D. Z. Ting, and E. T. Yu, J. Appl. Phys. **106**, 056101 (2009).
[9]D. Alonso-Álvarez, B. Alén, J. M. García, and J. M. Ripalda, Appl. Phys. Lett. **91**, 263103 (2007).
[10]D. Zhou, G. Sharma, S. F. Thomassen, T. W. Reenaas, and B. O. Fimland, Appl. Phys. Lett. **96**, 061913 (2010).
[11]R. B. Laghumavarapu, A. Moscho, A. Khoshakhlagh, M. El-Emawy, L. F. Lester, D. L. Huffaker, Appl. Phys. Lett. **90**, 173125 (2007).
[12]D. Guimard, R. Morihara, D. Bordel, K. Tanabe, Y. Wekayama, M. Nishioka, and Y. Arakawa, Appl. Phys. Lett. **96**, 203507 (2010).
[13]S. M. Hubbard, C .P. Cress, C. G. Bailey, R. P. Rafaelle, S. G. Bailey, and D. M. Witt, Appl. Phys. Lett. **92**, 123512 (2008).
[14]J. Wu, D. Shao, Z. Li, M. O. Manasreh, V. P. Kunets, Z. M. Wang, and G. J. Salamo, Appl. Phys. Lett. **95**, 071908 (2009).
[15]Y. Okada, T. Morioka, K. Yoshida, R. Oshima, Y. Shoji, T. Inoue, and T. Kita, J. Appl. Phys. **109**, 024301 (2011).
[16]B. Lita, R. S. Goldman, J. D. Phillips, and P. K. Bhattacharya, Appl. Phys. Lett. **75**, 2797 (1999).
[17]B. Lita, R. S. Goldman, J. Phillips, P. K. Bhattacharya, Appl. Phys. Lett. **74**, 2824 (1999).
[18]L. R. C. Fonseca, J. L. Jimenez, and J. P. Leburton, Phys. Rev. B **58**, 9955 (1998).
[19]W. Ye, S. Hanson, X. Weng, and R. S. Goldman, J. Vac. Sci. Technol. B **23**, 1736 (2005).
[20]V. D. Dasika, R. S. Goldman, J. D. Song, W. J. Choi, I. K. Han, and J. I. Lee, J. Appl. Phys. **106**, 014315 (2009).
[21]C. G. Van de Walle, Phys. Rev. B **39**, 1871 (1989).
[22]V. Aroutiounian, S. Petrosyan, and A. Khachatryan, J. Appl. Phys. **89**, 2268 (2001).
[23]S. L. Chuang, *Physics of Photonic Devices* (Wiley, New York, 2009), p. 821.
[24]P. R. Bevington, in *Data Reduction and Error Analysis for the Physical Sciences* (McGraw-Hill, New York, 1969), p. 110.
[25]H. Shin, E. Yoon, K.-S. Hong, W. Lee, Y.-H. Yoo, Appl. Phys. A **81**, 715 (2005).

Downloaded 28 Jun 2013 to 141.211.173.82. This article is copyrighted as indicated in the abstract. Reuse of AIP content is subject to the terms at: http://jap.aip.org/about/rights_and_permissions